IOPscience iopscience.iop.org

Home Search Collections Journals About Contact us My IOPscience

Nanocomposite scaffolds with tunable mechanical and degradation capabilities: co-delivery of bioactive agents for bone tissue engineering

This content has been downloaded from IOPscience. Please scroll down to see the full text.

2016 Biomed. Mater. 11 065003

(http://iopscience.iop.org/1748-605X/11/6/065003)

View the table of contents for this issue, or go to the journal homepage for more

Download details:

IP Address: 157.92.4.6
This content was downloaded on 01/12/2016 at 17:44

Please note that terms and conditions apply.

You may also be interested in:

A bioceramic with enhanced osteogenic properties to regulate the function of osteoblastic and osteocalastic cells for bone tissue regeneration
Seyed-Iman Roohani-Esfahani, Young Jung No, Zufu Lu et al.

The effects of injectable calcium silicate-based composites with the Chinese herb on an osteogenic accelerator in vitro
Nai-Jen Chang, Yi-Wen Chen, Den-En Shieh et al.

The synergistic effect of VEGF and biomorphic silicon carbides topography on in vivo angiogenesis and human bone marrow derived mesenchymal stem cell differentiation
P Díaz-Rodríguez, J L Gómez-Amoza and M Landin

Injectable osteogenic and angiogenic nanocomposite hydrogels for irregular bone defects
M Vishnu Priya, A Sivshanmugam, A R Boccaccini et al.

Preparation and in vitro evaluation of strontium-doped calcium silicate/gypsum bioactive bone cement
Juncheng Wang, Lei Zhang, Xiaoliang Sun et al.

Enhanced angiogenesis and osteogenesis in critical bone defects by the controlled release of BMP-2 and VEGF: implantation of electron beam melting-fabricated porous Ti6Al4V scaffolds incorporating growth factor-doped fibrin glue
Jia Lv, Peng Xiu, Jie Tan et al.

Angiogenesis stimulated by novel nanoscale bioactive glasses
Cong Mao, Xiaofeng Chen, Guohou Miao et al.

Biomedical Materials

PAPER

Nanocomposite scaffolds with tunable mechanical and degradation capabilities: co-delivery of bioactive agents for bone tissue engineering

RECEIVED
20 February 2016

REVISED
20 August 2016

ACCEPTED FOR PUBLICATION
2 September 2016

PUBLISHED
21 October 2016

Juan P Cattalini[1], Judith Roether[2], Alexander Hoppe[3], Fatemeh Pishbin[4], Luis Haro Durand[5], Alejandro Gorustovich[5], Aldo R Boccaccini[3], Silvia Lucangioli[1,5] and Viviana Mouriño[1,5]

[1] Department of Pharmaceutical Technology, Faculty of Pharmacy and Biochemistry, University of Buenos Aires, Buenos Aires, PC1113, Argentina
[2] Department of Materials Science and Engineering, Institute of Polymer Materials, University of Erlangen-Nuremberg, Erlangen, 91058, Germany
[3] Department of Materials Science and Engineering, Institute of Biomaterials, University of Erlangen-Nuremberg, Erlangen, 91058, Germany
[4] Department of Materials, Imperial College London, London, SW7 2AZ, UK
[5] National Research Council (CONICET), Buenos Aires, Argentina

E-mail: vmourino@ffyb.uba.ar

Keywords: nanocomposite scaffolds, bone tissue engineering, controlled and sustainable release, ions, alendronate delivery

Abstract

Novel multifunctional nanocomposite scaffolds made of nanobioactive glass and alginate crosslinked with therapeutic ions such as calcium and copper were developed for delivering therapeutic agents, in a highly controlled and sustainable manner, for bone tissue engineering. Alendronate, a well-known antiresorptive agent, was formulated into microspheres under optimized conditions and effectively loaded within the novel multifunctional scaffolds with a high encapsulation percentage. The size of the cation used for the alginate crosslinking impacted directly on porosity and viscoelastic properties, and thus, on the degradation rate and the release profile of copper, calcium and alendronate. According to this, even though highly porous structures were created with suitable pore sizes for cell ingrowth and vascularization in both cases, copper-crosslinked scaffolds showed higher values of porosity, elastic modulus, degradation rate and the amount of copper and alendronate released, when compared with calcium-crosslinked scaffolds. In addition, in all cases, the scaffolds showed bioactivity and mechanical properties close to the endogenous trabecular bone tissue in terms of viscoelasticity. Furthermore, the scaffolds showed osteogenic and angiogenic properties on bone and endothelial cells, respectively, and the extracts of the biomaterials used promoted the formation of blood vessels in an *ex vivo* model. These new bioactive nanocomposite scaffolds represent an exciting new class of therapeutic cell delivery carrier with tunable mechanical and degradation properties; potentially useful in the controlled and sustainable delivery of therapeutic agents with active roles in bone formation and angiogenesis, as well as in the support of cell proliferation and osteogenesis for bone tissue engineering.

1. Introduction

The fabrication of 3D scaffolds for bone tissue engineering (BTE) is focused on achieving a suitable material in terms of bioactivity, biocompatibility and mechanical properties, as well as an interconnected porous structure in order to support, reinforce and organize the new bone tissue in-growth and regeneration [1]. In addition, the fabrication of multifunctional scaffolds gives an added value since matrices could be used as structures not only to support bone tissue growth, but to lead and control bone regeneration [2–4]. In this regard, it is interesting to use the scaffold to deliver different agents that play important roles in osteogenesis and angiogenesis to encourage the integration between the biomaterials and the tissue to be regenerated [5–7]. In a previous work, new nanocomposite biomaterials made of bioactive glass nanoparticles (Nbg) and alginate crosslinked with different cations have been developed to fabricate scaffolds for BTE [8–11]. The fact of developing novel nanocomposite biomaterials with

© 2016 IOP Publishing Ltd

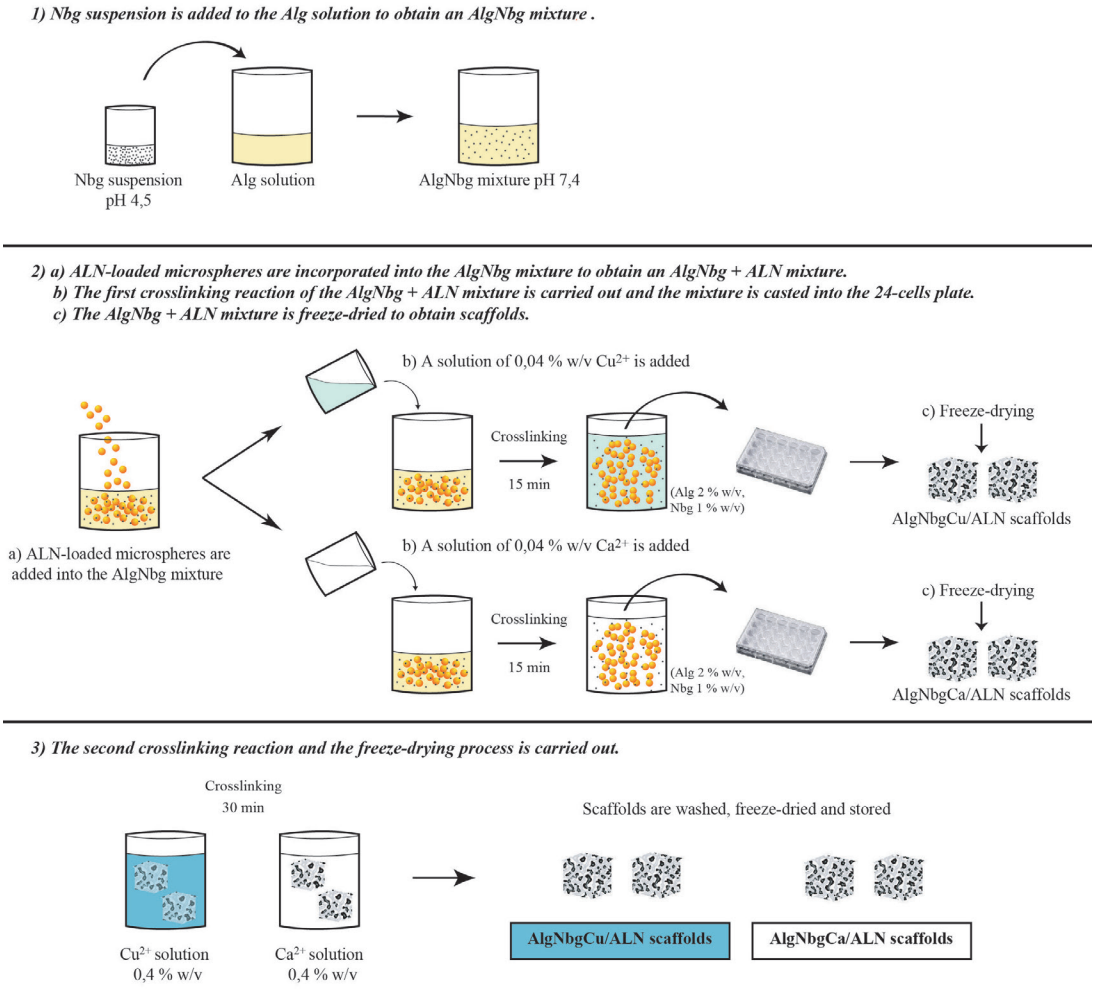

Figure 1. This figure shows the method of preparation of AlgNbgCu/ALN and AlgNbgCa/ALN scaffolds.

suitable properties in terms of biodegradability, bioactivity, biocompatibility, mechanical strength and *in vitro* angiogenesis and osteogenesis, prompted us to use them for the elaboration of engineered scaffolds as multifunctional platforms for bone tissue regeneration. In this sense, metallic ions as therapeutics agents (MITA) such as calcium (Ca^{2+}) and copper (Cu^{2+}) have been used to develop these new nanocomposite biomaterials previously mentioned [8] due to their roles in bone formation [6, 12] and the angiogenic effect of (Cu^{2+}) [12–14]. Moreover, the possibility to incorporate therapeutic agents into the scaffolds for the treatment of bone diseases would enhance their functionality [15–17]. In this regard, antiresorptive agents such as bisphosphonates (BPs) have been extensively used for the oral and parenteral treatment of bone disorders such as Paget's disease, osteoporosis, hyperkalaemia of malignancy, osteogenesis imperfect, and inflammation related bone loss, to promote fracture repair [18, 19]. However, the low bioavailability after oral administration and the associated side effects as well as adverse reactions related with parenteral administration are very well known drawbacks of BPs [20, 21]. Therefore, the possibility to deliver BPs at the desired site of activity as well as to achieve therapeutic concentration levels would allow us to obtain a high specific response [22–24]. Several reports have shown the advantages of incorporating BPs into scaffolds for BTE: the inhibition of the recruitment and differentiation of osteoclast precursors and the resorptive activity of mature osteoclasts; induction of apoptosis of macrophages and mature osteoclasts; as well as the enhancement of the proliferation, differentiation, and bone-forming activity of osteoblasts [23]. According to these considerations, we aimed to prepare bioactive nanocomposite and multifunctional scaffolds with tunable mechanical and degradation capabilities, which could be able to co-deliver osteogenic, angiogenic and antiresorptive agents to promote bone regeneration and vascularization in a controlled and sustainable manner.

2. Materials and methods

2.1. Materials

Nbg with the nominal composition close to 45S5 *Bioglass*® (46 mol% SiO_2, 23 mol% Na_2O, 27 mol% CaO, 4 mol% P_2O_5), with spherical shape and mean particle size 35–40 nm (courtesy of D Mohn and Prof W Stark, Swiss Federal Institute of Technology

Zurich, Switzerland) were prepared by the flame spray method [25] and characterized [26]. Sodium alginate (Alg) (Protanal LF 10/60), was obtained from FMC Biopolymers. Alendronate sodium trihydrate (ALN) was obtained from Aryl S A (Argentina). Hydrochloride acid (HCl), monobasic sodium phosphate (NaH_2PO_4) and ammonium phosphate ($NH_4H_2PO_4$) were obtained from Sigma Aldrich (USA). $SO_4Cu \cdot 5H_2O$ was obtained from Fluka (USA) and $CaCl_2 \cdot 2H_2O$ from MERCK (Darmstadt, Germany). 24-wells plates were used to prepare the scaffolds (Corning® Costar®, Sigma, Argentina).The water used was purified by distillation and deionization (MilliQ).

2.2. Methods

2.2.1. Preparation and characterization of alendronate-loaded microspheres

Microspheres were prepared by an ionic crosslinking technique [27]. A solution of a final concentration of 1% w/v and 0.5 mg ml^{-1} for Alg and ALN, respectively was added dropwise via a 20-gauge hypodermic needle fitted with a 10 ml syringe into a 50 mM $CaCl_2 \cdot 2H_2O$ solution. After the microspheres were formed, they were washed and dried until they maintained a constant weight at 37 °C for 24 h in an oven. The morphology and size of the microspheres were analyzed by an optical microscope (Arcano, China).

2.2.2. Alendronate encapsulation

The efficiency of the encapsulation of ALN (%E) was evaluated by the difference between the amount of ALN present at the Alg–ALN solution (C_i, initial concentration) and the amount of ALN present in the calcium chloride solution used during the microsphere preparation (C_f, final concentration). The following equation was used to calculate the encapsulation efficiency:

$$\%E = \frac{C_i - C_f}{C_i} \cdot 100$$

2.2.3. Preparation of nanocomposite scaffolds

The preparation technique of the scaffolds is shown schematically in figure 1. An aqueous dispersion of Nbg was added to an Alg solution previously prepared to obtain an AlgNbg mixture, which was adjusted to pH 7.4. ALN-loaded microspheres prepared as indicated in section 2.1 were incorporated into the AlgNbg mixture. Then, a solution of 0.04% w/v of Cu^{2+} or Ca^{2+} ions was added to the AlgNbg/ALN-loaded microsphere mixture in order to produce the first crosslinking reaction in order to achieve a final concentration of 2% w/v and 1% w/v for Alg and Nbg, respectively). After freezing at −20 °C for 24 h, the lyophilization was performed at −40 °C for 48 h (FIC L05 equipment, Argentina) to obtain the AlgNbgCu/ALN and AlgNbgCa/ALN scaffolds. Then, the scaffolds were crosslinked once more with a higher concentration solution of 0.4% w/v of Cu^{2+}or Ca^{2+} ions, respectively. Finally, the scaffolds were freeze-dried under the same conditions and cylindrical porous scaffolds with the size of 12.7 mm diameter and 12.5 mm height were obtained. In addition, scaffolds without Nbg were prepared by the same procedure: AlgCa/ALN and AlgCu/ALN. Moreover, scaffolds without ALN-loaded microspheres were also prepared: AlgNbgCa, AlgNbgCu, AlgCa and AlgCu.

2.2.4. Characterization of scaffolds

2.2.4.1. Morphology and porosity estimation

The morphology of the scaffolds and the pore sizes were analyzed by scanning electron microscope (SEM, Zeiss Leica, Germany). The porosity was measured by the displacement method [28]. Three samples of each scaffold (AlgNbgCu/ALN, AlgNbgCa/ALN, AlgNbgCu, AlgNbgCa, AlgCu and AlgCa) were immersed in distilled water and placed in a shaker at 37 °C and 60 rpm for 48 h (KS 40001 Control Shaker IKA, Germany). The porosity of the scaffolds was estimated as follows:

$$P = \frac{W_f - W_i}{\delta V_i} \cdot 100$$

where W_i and W_f represent the weight of the scaffolds before and after immersing them in distilled water, V_i is the volume of the scaffolds before immersing them in distilled water and δ is the constant density of water.

2.2.4.2. Mechanical characterization

The compressive strength of the AlgNbgCu/ALN, AlgNbgCa/ALN, AlgNbgCu and AlgNbgCa scaffolds was analyzed by a Zwick/Roell Z010 servohydraulic testing instrument. Dried samples were used and a cross-head speed of 0.5 mm min^{-1} with a preload of 1 kN was set. Five samples of each scaffold were used.

Dynamic mechanical thermal analyses (DMTA) were performed on the same scaffolds mentioned above, using a Rheometric Scientific DMTA Mark IV at 25 °C and a frequency sweep from 0.1–10 Hz. The DMTA analysis was performed on dried and wet scaffolds (before and after immersing them into phosphate buffer for 30 min). A preload of 325 and 50 g was used for the dried and wet scaffolds, respectively. Three samples of each scaffold were tested.

2.2.5. Bioactivity study

AlgNbgCu/ALN and AlgNbgCa/ALN scaffolds were immersed in simulated body fluid (SBF) [29], at 37 °C and 60 rpm for 15 d (KS 40001 Control Shaker IKA, Germany). After 7 and 15 d, the presence of hydroxyapatite crystals (HA) was confirmed by x-ray diffraction (XRD) using a D8 ADVANCE x ray diffractometer (Bruker, Madison, USA). In addition, the study was performed on the AlgCu/ALN and AlgCa/ALN scaffolds.

2.2.6. Degradation and swelling study

The degradation study of the AlgNbgCu/ALN and AlgNbgCa/ALN scaffolds was performed in phosphate

buffer (10 mM, pH 7.4). After 1, 7, 14, 21, 28, 43 and 56 d incubation at 37 °C, the samples were removed, washed, lyophilized and weighed. The weight loss percentage (%WL) was calculated as follows:

$$\%\mathrm{WL} = \frac{W_i - W_f}{W_i} \cdot 100$$

where W_i and W_f are the weight of the dried scaffolds before and after immersing them in buffer.

On the other hand, the swelling capacity was studied by analyzing the weight gain of the AlgNbgCu/ALN and AlgNbgCa/ALN scaffolds after 1, 2, 7 and 15 d of incubation in phosphate buffer (10 mM, pH 7.4) at 37 °C. The percentage weight gain (%WG) was calculated as follows:

$$\%\mathrm{WG} = \frac{W_f - W_i}{W_i} \cdot 100$$

where W_i is the weight of the scaffolds before immersing them in buffer, and W_f is the weight of the scaffolds after removing the excess of buffer with a filter paper. Three samples of each scaffold were tested in both studies.

2.2.7. Release profile of ALN, Cu^{2+} and Ca^{2+} from the scaffolds

The release of ALN, $Cu^{2+}$and Ca^{2+} ions from the AlgNbgCu/ALN and AlgNbgCa/ALN scaffolds, respectively, was studied in phosphate buffer (10 mM, pH 7.4) at 37 °C. Aliquots were withdrawn from the media at regular intervals (1, 7, 14, 21, 28, 43 and 58 d) and the scaffolds were re-immersed in fresh buffer. In addition, samples were taken during the first 2, 4, and 8 h for the quantification of Cu^{2+} and Ca^{2+} release. Quantification was made by capillary electrophoresis methods [30, 31].

2.2.8. In vitro studies

2.2.8.1. Preparation of biomaterial extracts

The intention of the *in vitro* studies was to prove the bioactivity of extracts in order to know the behavior of cells upon therapeutic ions and alendronate released in the context of the extracts obtained from the scaffold. Extracts of AlgNbgCu/ALN and AlgNbgCa/ALN scaffolds were prepared according to ISO 10993-12. Briefly, the scaffolds were incubated for 1, 14, 21, 43 and 58 d at 37 °C in low-glucose Dulbecco's modified Eagle medium (L-DMEM) (Hyclone, USA) or endothelial cell medium (ECM) (Sciencell, USA). The ratio of the scaffolds to the medium was 100 mg ml^{-1}. Cultures of the cells in the presence of a range of ionic concentrations of Cu^{2+} or Ca^{2+} introduced directly into the culture media were used as controls (ControlCu and ControlCa, respectively). The ion concentrations of Cu^{2+} or Ca^{2+} used were those obtained from the release studies according to section 2.2.8 for each period of incubation. Extracts of AlgCu/ALN and AlgCa/ALN were also prepared as control samples. Five samples of each type of scaffold were used and the extracts were renewed at each medium change during cell culture.

2.2.8.2. Cell preparation and culture

Rat bone marrow-derived mesenchymal stem cells (rBMSCs) were obtained from the femora of 4 week-old Sprague Dawley rats, as previously described [32]. Briefly, marrow of the femora midshaft was flushed out and suspended in L-DMEM supplemented with 10% fetal bovine serum (FBS, Hyclone, USA), 100 U ml^{-1} penicillin and 100 mg l^{-1} streptomycin (Hyclone, USA). Non-adherent cells were removed after 3 d. When approximately 80% confluence was reached, the cells were passaged and used for the following experiments from second to third passages.

Human umbilical vein endothelial cells (HUVECs) were isolated and cultured as described previously [13], with written informed consent of the donors. Briefly, the umbilical vein was digested with 0.1% collagenase I (Sigma, USA) for 15 min at 37 °C. Subsequently, the cells were collected and cultured in ECM (Sciencell, San Diego, USA). Non-adherent cells were removed after 24 h. HUVECs between the third and sixth passage were used in experiments.

2.2.8.3. Cell viability assays

Cell viability was evaluated by 3-(4,5-dimethylthiazol-2-yl)-2,5-diphenyltetrazolium bromide (MTT) colorimetric assay. Briefly, cells were seeded in 96-well plates at 3.1×10^4 cells cm^{-2}. The extracts described above, in section 2.2.8.1, were added, respectively, and incubated for 24 h. The MTT assay (Sigma, USA) was performed following the manufacturer's instructions. Dimethyl sulfoxide (DMSO, Sigma, USA) was used to dissolve the formazan crystals, and the optical density was measured at 570 and 630 nm using a microplate reader (Labsystems Dragon Wellscan MK3, Finland).

2.2.8.4. Alkaline phosphatase staining and activity assay

Alkaline phosphatase (ALP) staining was performed using a BCIP/NBT ALP kit (Beyotime, Shanghai, China). Briefly, the rBMSCs were plated in 6-well plates and cultured for 10 d with different extracts as indicated in section 2.2.8.1. After fixation with 4% paraformaldehyde, the cells were incubated in a mixture of nitro-blue tetrazolium and 5-bromo-4-chloro-3-indolylphosphate [33]. ALP activity was assessed using an ALP Detection Kit (Jiancheng Technology, Nanjing, China). Control samples were also assayed. The ALP activity was examined according to the manufacturer's instructions and normalized to the total protein content determined using the BCA method, as previously described [34].

2.2.9. Ex vivo study on chorioallantoic membrane

2.2.9.1. Preparation of biomaterial extracts

An *ex vivo* study using the chorioallantoic membrane (CAM) of quail eggs was performed to evaluate the angiogenic properties of AlgNbgCu scaffolds [35–37]. Briefly, the scaffolds were incubated in free calcium and

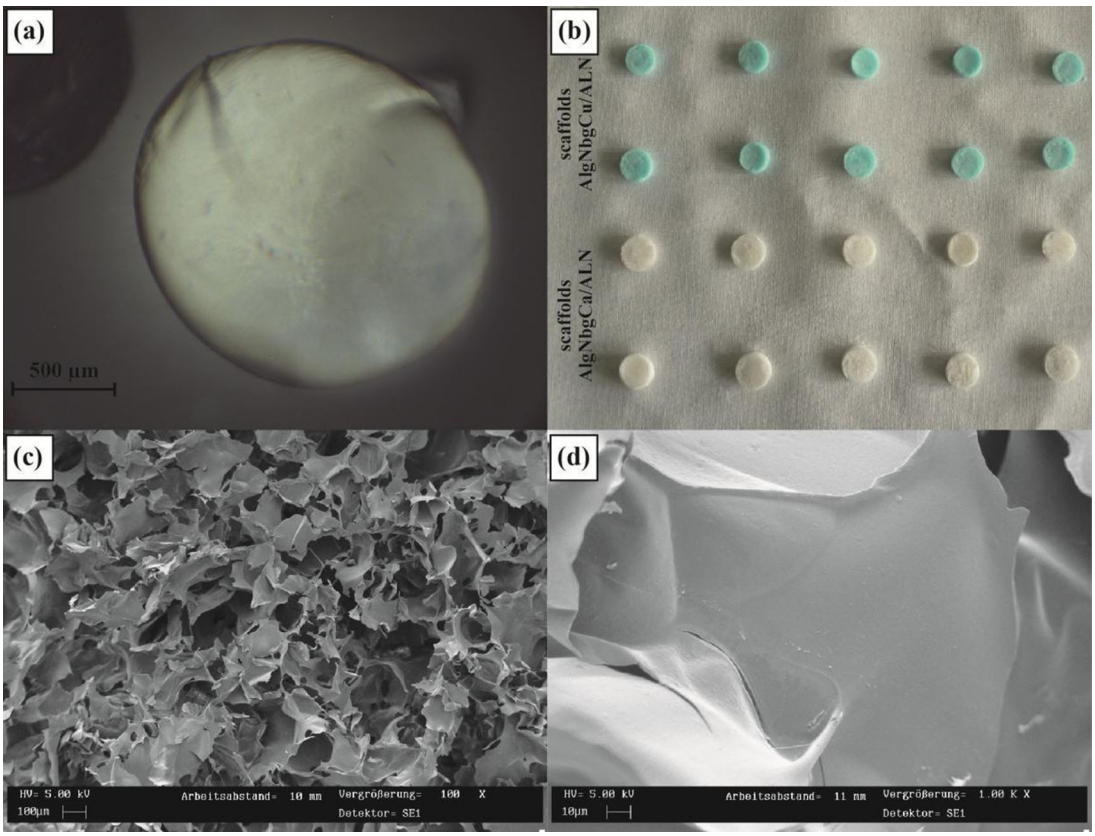

Figure 2. (a) Picture of ALN-loaded microspheres before drying for their use in scaffold fabrication. (b) This figure shows the morphology of AlgNbgCu/ALN (top) and AlgNbgCa/ALN (bottom) scaffolds after preparation. (c) SEM image showing the microstructure of the inner part of the nanocomposite scaffolds. (d) SEM image of the pore wall surface at higher magnification. Samples shown from the AlgNbgCu/ALN scaffolds.

magnesium Hank's balanced salt solution (HBSS) at 37 °C for 24 h. Then, discs made of filter paper were immersed in the solution that was previously used for scaffold incubation.

2.2.9.2. Quail eggs chorioallantoic membrane preparation
Fertile quail eggs (*C. coturnix*) were used and kept *in ovo* in an incubator for 72 h at 37 °C and 60% relative humidity. Then, a part of the shell was removed and embryos were placed into 6-well plates (in order to perform an *ex ovo* study), containing distilled water, at 37 °C for 7 d to allow the CAM to cover 80% of the well surface. No antibiotics or culture medium were added to the wells [35–37].

2.2.9.3. Effect of 2D AlgNbgCu/ALN scaffold extracts on blood vessel formation
After the incubation of the CAM, paper filter discs impregnated with the conditioned HBSS mentioned previously were placed on the CAM. After 48 h, the embryos were sacrificed and the CAM was fixed in paraformaldehyde and glutaraldehyde solution (4 and 2% v/v, respectively). The fixation was performed for 48 h. The CAM was subsequently dried and analyzed by a stereoscopic microscope to determine the number of blood vessels formed (called branch points) on the CAM area that was in contact with the impregnated discs. The CAM treated with basic fibroblast growth factor (bFGF) was used as a positive control group, untreated CAM was used as a control group, and the effect of the control groups and 2D AlgNbgCu/ALN scaffold extracts was compared with the effect produced by the 2D Alg scaffold.

2.2.10. Statistical analysis
All quantitative results were obtained from assays using three or five samples. Data was expressed as the mean ± standard deviation (SD). The Student's *t*-test was used for statistical analysis. A value of $p < 0.05$ was considered to be statistically significant. ANOVA was used for comparing data from studies.

3. Results

3.1. Characterization and encapsulation efficiency of ALN-loaded microspheres
The encapsulation efficiency of the ALN-loaded microspheres obtained was 98.7 ± 0.1%. The size of the microspheres was 1.7 ± 0.1 mm, and the morphology is shown in figure 2(a). After drying the microspheres, the size was 890 ± 12 μm.

3.2. Characterization of scaffolds
3.2.1. Morphology and porosity
AlgNbvCu/ALN scaffolds were obtained with 12.2 mm diameter and 12.0 mm height, whereas AlgNbvCa/ALN scaffolds were obtained with 13.3 mm diameter

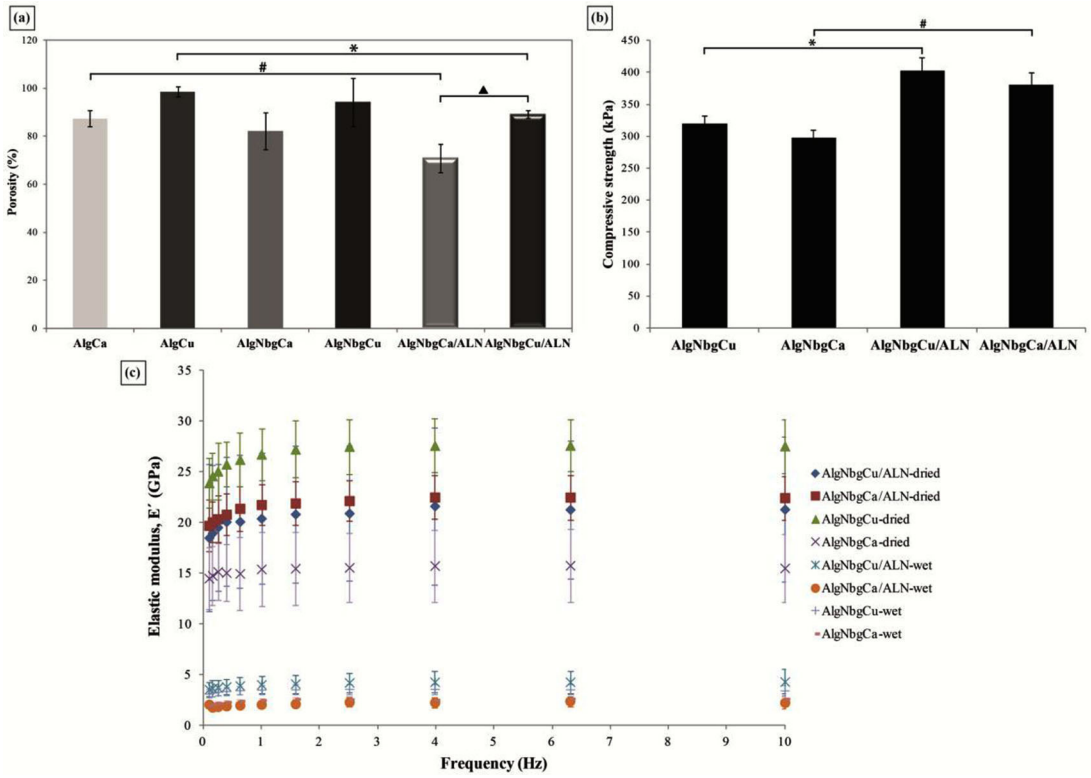

Figure 3. (a) AlgNbgCu/ALN scaffolds showed a porosity of 90 ± 2%, whereas AlgNbgCa/ALN scaffolds showed a porosity of 71 ± 6%. The incorporation of Nbg within the scaffolds did not seem to affect their porosity, but when both Nbg and ALN-loaded microspheres were incorporated, a significant decrease in the porosity was observed compared to the AlgCu and AlgCa scaffolds. This is significantly different ($p < 0.05$) from the #AlgCa, *AlgCu and ▲AlgNbvCa/ALN groups. (b) The incorporation of ALN-loaded microspheres produced a significant increase in the compressive strength of the AlgNbgCu/ALN and AlgNbgCa/ALN scaffolds in comparison with the AlgNbgCu and AlgNbgCa scaffolds. This is significantly different ($p < 0.05$) from the *AlgNbgCu and #AlgNbgCa groups. (c) The scaffolds showed no evident variations in the E' value along the frequency sweep ($p > 0.05$). It can be noted that the dried samples showed E' values significantly higher ($p < 0.05$)—about 15–30 GPa, in comparison with the wet samples—about 2–5 GPa. The data are presented as average values ±SD in all graphics.

and 12.5 mm height; their morphologies are shown in figures 2(b)–(d). The pore sizes of the scaffolds were from several microns (200–300 μm) to a few hundred microns. The estimated porosity of the scaffolds is presented in figure 3(a). The incorporation of Nbg within the AlgCu and AlgCa scaffolds did not seem to affect their porosity, and no significant decrease in the porosity value could be observed when we compared the AlgCu and AlgCa with AlgNbgCu and AlgNbgCa scaffolds, respectively ($p > 0.05$). In addition, the incorporation of ALN-loaded microspheres within the AlgNbvCu and AlgNbvCa scaffolds did not decrease significantly the porosity ($p > 0.05$) when we compared the AlgNbgCu/ALN and AlgNbgCa/ALN scaffolds with AlgNbgCu and AlgNbgCa scaffolds, respectively. However, scaffolds containing Nbg and ALN-loaded microspheres, the AlgNbgCu/ALN and AlgNbgCa/ALN scaffolds, have shown a significant decrease in their porosity ($p < 0.05$) in comparison with the AlgCu and AlgCa scaffolds, respectively. Moreover, the porosity of the AlgNbgCu/ALN scaffolds (89 ± 2%) is significantly higher ($p < 0.05$) compared to that of the AlgNbgCa/ALN scaffolds (71 ± 6%).

3.2.2. *Mechanical properties*

As it is shown in figure 3(b), the compressive strength of the AlgNbgCu/ALN and AlgNbgCa/ALN scaffolds increased significantly in comparison with scaffolds without ALN-loaded microspheres (AlgNbgCu and AlgNbgCa scaffolds). The values of the compressive strength for the AlgNbgCu/ALN and AlgNbgCa/ALN scaffolds were 402 ± 21 kPa and 381 ± 18 kPa, respectively. The storage modulus (elastic modulus, E') is shown in figure 3(c) as a function of frequency. When the dried and wet samples are compared, the E' value from the dried samples is significantly higher ($p < 0.05$). In general, dried samples showed values within the range 15–30 GPa, whereas wet samples showed values from 2–5 GPa. With regard to the dried samples, the E' value for the AlgNbgCu scaffolds was significantly higher than that of the AlgNbgCa scaffolds ($p < 0.05$). However, after the addition of the ALN-loaded microspheres no significant difference in the E' value was observed, when we compared the AlgNbgCu/ALN and AlgNbgCa/ALN scaffolds with the AlgNbvCu and AlgNbvCa scaffolds, respectively ($p > 0.05$). Moreover, the incorporation of ALN-loaded microspheres produced a significant increase ($p < 0.05$) in the E' value for those nanocomposite scaffolds crosslinked with Ca^{2+} compared with the AlgNbgCa samples without ALN-loaded microspheres, whereas there was a significant decrease ($p < 0.05$) in the E' value

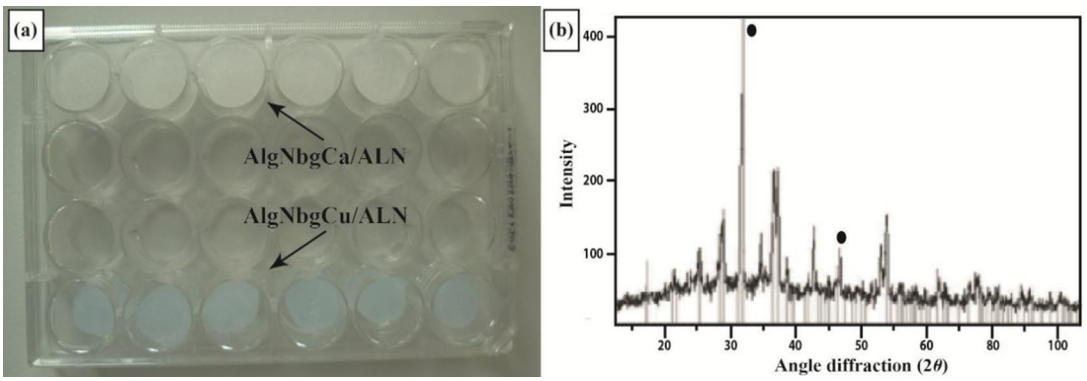

Figure 4. (a) Aspect of the AlgNbgCa/ALN and AlgNbgCu/ALN scaffolds after 7 d of immersion in SBF. (b) XRD spectra showing characteristic peaks at 31.8° and 46.7° from HA crystals deposited on the scaffold surface (the spectra shown in this figure were obtained for the AlgNbgCu/ALN scaffolds, and similar results were found for the AlgNbgCa/ALN scaffolds).

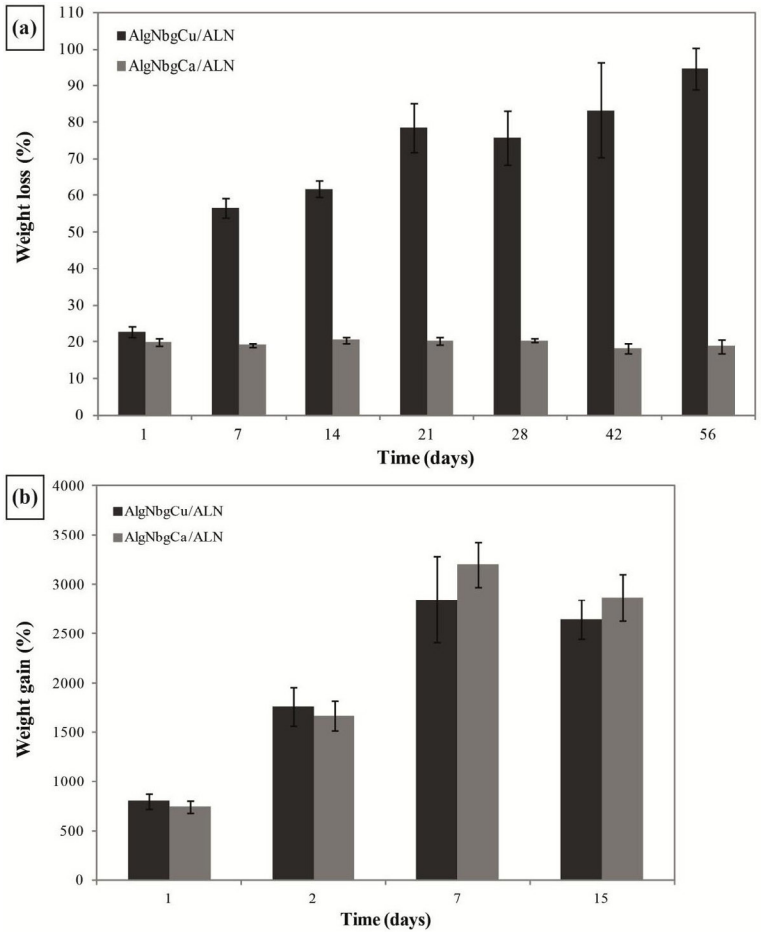

Figure 5. (a) No significant variations in the weight loss were observed for the AlgNbgCa/ALN scaffolds, and they degraded at a slower rate showing a %WL of 20 ± 1%. The AlgNbgCu/ALN scaffolds degraded at a higher rate, which was more noticeable after the first week, reaching a %WL of 95 ± 6% by the end of the study. (b) Values greater than 100% were observed in terms of weight gain after 1 d until the end of the assay for the AlgNbgCa/ALN and AlgNbgCu/ALN scaffolds. The data are presented as average values ±SD.

for those nanocomposite scaffolds crosslinked with Cu^{2+} compared to the AlgNbgCu samples without ALN-loaded microspheres.

On the other hand, the results from the wet samples showed that the E' value was significantly higher for nanocomposite scaffolds crosslinked with Cu^{2+} than that of those crosslinked with Ca^{2+} ($p < 0.05$). In addition, no significant difference was observed in the E' value, whether or not ALN-loaded microspheres were present in the scaffolds ($p > 0.05$).

3.3. Bioactivity study

Figure 4(a) shows the aspect of the AlgNbgCa/ALN and AlgNbgCu/ALN scaffolds after 7 d of immersion in SBF. After 15 d of immersion in SBF, the presence of HA in the surface of the scaffolds was confirmed by XRD,

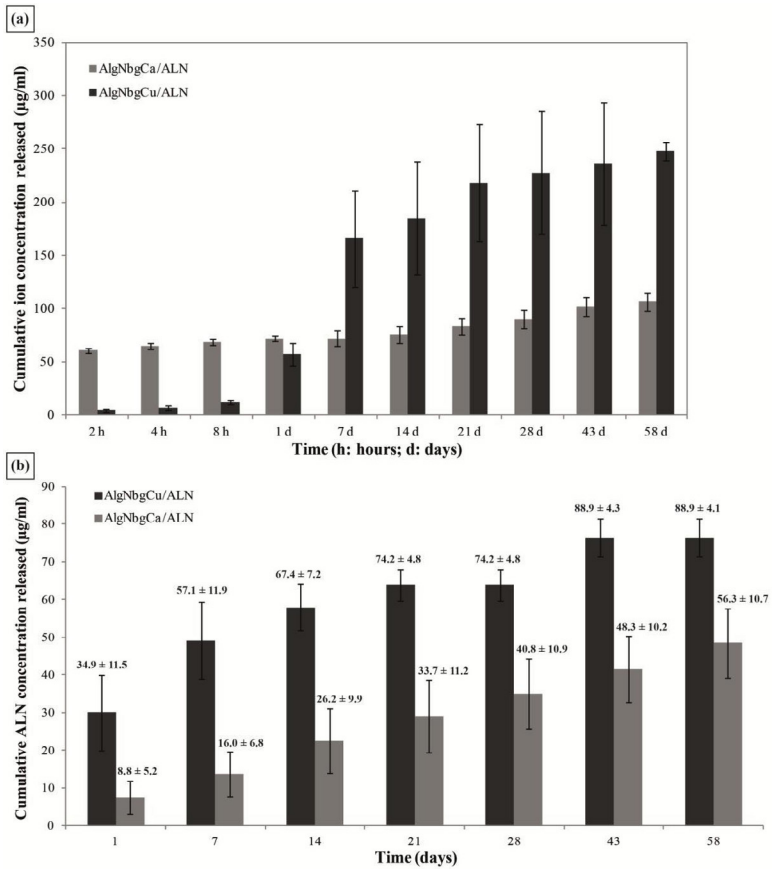

Figure 6. (a) Release profile of Cu^{2+} and Ca^{2+} ions. The amount of Cu^{2+} and Ca^{2+} ions released from AlgNbgCu/ALN and AlgNbgCa/ALN, respectively, increased during the time frame studied. For Cu^{2+} ions, while low concentrations were released during the first week of the study, a significant increase in the amount released was observed ($p < 0.01$) after day 7. On the other hand, the release profile of Ca^{2+} indicated that those ions were released in a constant and sustained manner during the whole time frame studied. From day 7 until the end of the study, the release profile of the cations showed that the amount of Cu^{2+} ions released from the AlgNbgCu/ALN scaffolds was higher than that of Ca^{2+} ions released from the AlgNbgCa/ALN scaffolds. The data are presented as average values ±SD. (b) ALN release profile from the scaffolds. AlgNbgCu/ALN scaffolds released a significantly higher concentration of ALN than AlgNbgCa/ALN scaffolds ($p < 0.05$) in each time frame studied. The cumulative concentration of ALN released from the AlgNbgCu/ALN and AlgNbgCa/ALN scaffolds was 76 ± 5 and 48 ± 9 $\mu g\ ml^{-1}$, respectively, which represents 89 ± 4% and 56 ± 11%, respectively, of the total amount of ALN incorporated within those scaffolds. The percentages of ALN released are indicated at the top of each graph bar. The data are presented as average values ±SD.

where the spectra (figure 4(b)) showed sharp peaks at 31.8° and 46.7° attributed to the 211 and 222 plane of HA [38, 39].

3.4. Degradation and swelling study

The degradation profile of the AlgNbgCu/ALN and AlgNbgCa/ALN scaffolds is shown in figure 5(a). The AlgNbgCa/ALN scaffolds remained shaped from the beginning until the end of the study and showed, on average, a %WL of 20 ± 1% by the end of the study. In addition, no significant variations in the weight loss were observed between the time frames studied ($p > 0.05$). In contrast, the AlgNbgCu/ALN scaffolds degraded at a significantly higher rate than the AlgNbgCa/ALN scaffolds ($p < 0.01$), which was more noticeable after the first week of the study. After 7 and 14 d, the AlgNbgCu/ALN scaffolds showed (on average) a %WL of 57 ± 3% and 62 ± 2%, respectively, and then the degradation percentage increased until it reached a value of 95 ± 6% by the end of the study.

The swelling ability of the scaffolds is shown in figure 5(b). It can be observed that the AlgNbgCu/ALN and AlgNbgCa/ALN scaffolds took up water more than their own weight since the beginning of the study. A significant increase ($p < 0.01$) in the %WG was observed in each time frame studied (from day 1 to 15) in comparison with the initial weight of the scaffolds. The %WG is higher than 100% since the beginning of the study. After 1, 2 and 7 d, a significant increase in %WG was observed, whereas no significant differences were observed when we compared results from 7 and 15 d ($p > 0.05$). In addition, any significant differences were observed between the swelling capacity of the AlgNbgCu/ALN and AlgNbgCa/ALN scaffolds.

3.5. Ions release profile

Figure 6(a) shows the concentration of $Cu^{2+}$and Ca^{2+} ions released as a function of time.

The amount of Cu^{2+} ions released from the AlgNbgCu/ALN scaffolds as well as the amount of Ca^{2+} ions released from the AlgNbgCa/ALN scaffolds increased

during the study, and the cumulative ion concentration released by the end of the assay was 248 ± 9 and 106 ± 8 μg ml^{-1}, respectively. In particular, the amount of Cu^{2+} ions released from the AlgNbgCu/ALN scaffolds was significantly lower than that of Ca^{2+} ions released from the AlgNbgCa/ALN scaffolds ($p < 0.01$) during the first 8 h of the study. After 7 d, a major increase in the release of Cu^{2+} ions was observed. From this time until the end of the study, the amount of Cu^{2+} released was significantly higher than that of Ca^{2+} ions in each time frame assayed ($p < 0.01$). On the other hand, the release profile of Ca^{2+} ions did not show any major increase in the amount of Ca^{2+} ions released, but a steady increase in each time frame was observed indicating a controlled and sustained release profile.

3.6. Alendronate release profile

Figure 6(b) shows the release profile of ALN from the AlgNbgCu/ALN and AlgNbgCa/ALN scaffolds. The amount of ALN released from the AlgNbgCu/ALN scaffolds was significantly higher than that released from the AlgNbgCa/ALN scaffolds ($p < 0.05$). After 7 d, the concentration of ALN released from the AlgNbgCu/ALN scaffolds was 49 ± 10 μg ml^{-1}, which is 57 ± 12% of the total amount of ALN incorporated within the scaffolds. From day 14 and until the end of the study, the increase in the amount of ALN released from the AlgNbgCu/ALN scaffolds in each time frame was lower in comparison with the increase observed in the amount of ALN released after 1 and 7 d. AlgNbgCu/ALN scaffolds released 76 ± 5 μg ml^{-1} of ALN, which is 89 ± 4% of the total amount of ALN incorporated within the scaffolds. On the other hand, the amount of ALN released from the AlgNbgCa/ALN scaffolds increased steadily in each time frame of the study. After 2 mo, the AlgNbgCa/ALN scaffolds released 48 ± 9 μg ml^{-1} of ALN, which is 56 ± 11% of the total amount of ALN incorporated within the scaffolds.

3.7. *In vitro* cellular studies

3.7.1. *Proliferation of rBMSCs cultured with AlgNbgCu/ALN and AlgNbgCa/ALN scaffold extracts*

rBMSCs treated with extracts of AlgNbgCu/ALN and AlgNbgCa/ALN scaffolds were the most metabolically active ($p < 0.005$) when compared to the ion concentration of calcium or copper, respectively, obtained from the release studies (see above, section 3.5) for each period of incubation and when compared to the AlgCu/ALN and AlgCa/ALN scaffolds, respectively. In addition, the extracts of the AlgCu/ALN and AlgCa/ALN scaffolds did not significantly affect cell metabolic activity and growth compared to L-DMEM. No significant differences in cell metabolic activity were observed for cells cultured in the extracts of the AlgNbgCu/ALN and AlgNbgCa/ALN scaffolds for the periods studied. Figure 7(a) shows the results for rBMSCs treated with extracts of the AlgNbgCu/ALN and AlgNbgCa/ALN scaffolds obtained after 24 h of soaking.

3.7.2. *Osteogenic differentiation of rBMSCs cultured with AlgNbgCu/ALN and AlgNbgCa/ALN scaffold extracts*

To investigate whether AlgNbgCu/ALN and AlgNbgCa/ALN scaffold extracts could affect the osteogenic differentiation of rBMSCs, ALP activity was examined. Interestingly, a time-dependent increase in ALP activity was observed for cells cultured in the extracts of the AlgNbgCu/ALN and AlgNbgCa/ALN scaffolds in the absence of osteogenic factors. ALP activity was not significantly different when the effect of the extracts from the AlgNbgCu/ALN and AlgNbgCa/ALN scaffolds were compared to the ones of the ion concentrations of Cu^{2+} and Ca^{2+} ions, respectively, obtained from the release studies (see above, section 3.5) for each period of incubation and when compared to the ones from the extracts of the AlgCu/ALN and AlgCa/ALN scaffolds, respectively, at day 3. However, ALP activity was significantly higher ($p < 0.001$) in cells cultured with the extracts of the AlgNbgCu/ALN and AlgNbgCa/ALN scaffolds after 10 d (figure 7(b)). No significant differences in ALP activity were observed for cells cultured in the extracts of the AlgNbgCu/ALN and AlgNbgCa/ALN scaffolds.

3.7.3. *Effect of AlgNbgCu/ALN and AlgNbgCa/ALN scaffold extracts on HUVECs function*

To understand the interactions of the AlgNbgCu/ALN and AlgNbgCa/ALN scaffold extracts with HUVECs, cell proliferation was analyzed. A significant increase of cell viability ($p < 0.005$) was observed when incubated with the AlgNbgCu/ALN and AlgNbgCa/ALN scaffold extracts obtained at different timepoints of material incubation, as per the details in the section Methods, 2.2.8.1—compared to the AlgCu/ALN and AlgCa/ALN scaffold extracts, respectively; to ControlCu and ControlCa, respectively; and the control. Figure 8 shows the results obtained when HUVEC cells were in contact with the AlgNbgCu/ALN and AlgNbgCa/ALN scaffold extracts collected after 24 h of incubation compared to the AlgCu/ALN and AlgCa/ALN scaffold extracts, respectively, and the control; although similar results were observed at each timepoint of material incubation. Furthermore, significantly higher cell viability was observed for the AlgNbgCu/ALN group compared to the AlgNbgCa/ALN group ($p < 0.001$).

3.8. *Ex vivo* study on chorioallantoic membrane

The extracts of 2D AlgNbgCu/ALN scaffolds produced a greater number of branch points on the CAM (figure 9) when compared with the effect of the control group and 2D Alg scaffold extracts ($p < 0.01$).

4. Discussion

The pore size and porosity obtained are within the range considered suitable for cell proliferation and blood vessel formation according to previous research [4, 40]. The pore size and morphology is important for

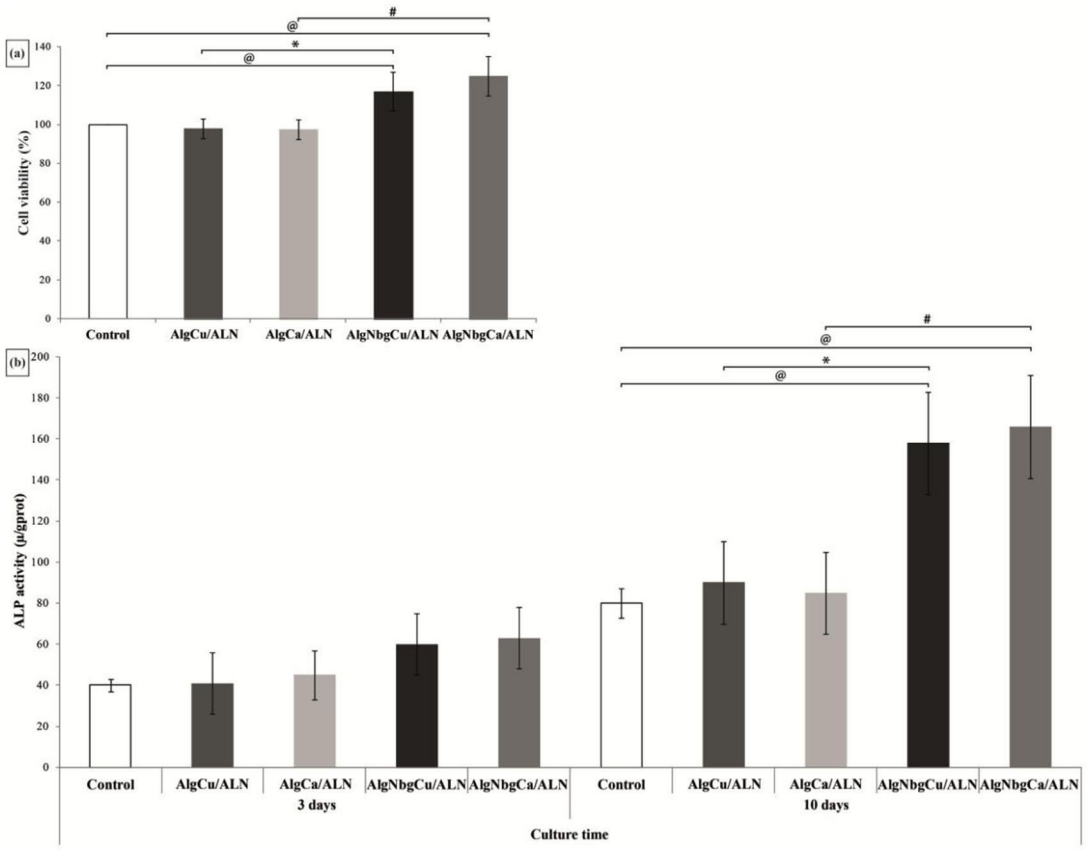

Figure 7. (a) The viability of rBMSCs after being in contact for 24 h with the extracts from the scaffolds. (b) Effects of the extracts on ALP activity of rBMSCs after 3 and 10 d. This is significantly different ($p < 0.05$) from @L-DMEM, AlgCa/ALN and *AlgCu/ALN groups. Cells in contact with L-DMEM were used as a control group. The results from ControlCu and ControlCa are not shown in the graphics. The scaffolds were incubated for 24 h at 37 °C in L-DMEM (see the text for more details about other incubation periods). The data are presented as average values ±SD.

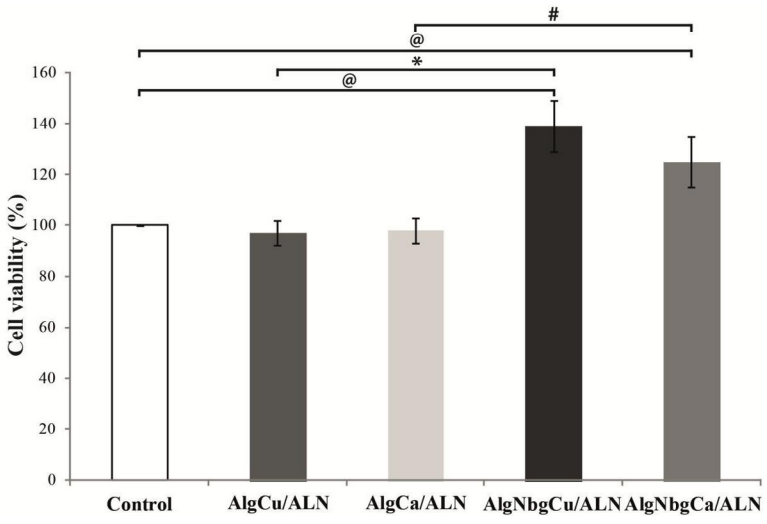

Figure 8. Effects of the extracts on HUVEC viability after 24 h of incubation. Significantly different ($p < 0.05$) from @ECM, #AlgCa/ALN and *AlgCu/ALN groups. The results from ControlCu and ControlCa are not shown in the graphics. The data are presented as average values ±SD.

nutrient diffusion and the removal of metabolic waste [40], and several works have reported that pore sizes from 200–350 μm are appropriate for cell invasion and blood vessel growth in BTE [40]. The pore size of the nanocomposite scaffolds developed is between 200 and 300 μm, and the porosity of the AlgNbgCu/ALN scaffolds was about 90%, whereas for the AlgNbgCu/ALN scaffolds it was about 70%. These results are in full compliance with previous works indicating that the pore size and porosity obtained are suitable for cell proliferation and blood vessel formation [4]. In addition, the porous structures obtained were similar

to trabecular bone tissue. A significant decrease in the porosity was observed for the AlgNbgCu/ALN and AlgNbgCa/ALN scaffolds compared to the AlgCu and AlgCa scaffolds, respectively, which could be attributed to the addition of Nbg [41], but also due to the incorporation of ALN-loaded microparticles. In addition, the fact that the AlgCu and AlgNbgCu/ALN scaffolds showed higher porosity compared to the AlgCa and AlgNbgCa/ALN scaffolds suggests that the radius of the cation influence is because of the way in which they interact with the Alg residues, giving rise to two types of matrices with different behaviors. Regarding the DMTA, the E' values of the scaffolds tested were compared in a frequency range of 0.1–10 Hz, which is the physiological frequency range of normal human activities from a slow walk to running in sports [42]. The results from the DMTA showed no evident variations along the frequency sweep for all samples tested, which indicates that the viscoelastic properties of the scaffolds are quite steady within a large time-scale range. In particular, the wet samples exhibited elastic modulus values similar to trabecular bone [43, 44], which is quite promising for BTE applications. The fact that both the dried and wet scaffolds crosslinked with Cu^{2+} ions showed higher elastic modulus values in comparison with those crosslinked with Ca^{2+} ions, except for the dried scaffolds containing ALN-microspheres, suggests that the size of the cation influences the mechanical properties, probably due to the way in which they interact with the Alg residues. These results might be related to what was observed after the scaffold preparation: the Cu^{2+}-crosslinked scaffolds showed a harder and more shrunken structure after being prepared than the Ca^{2+}-crosslinked scaffolds, which could explain—at least partially—the results obtained from DMTA. The bioactive character of the nanocomposite scaffolds tested would allow the deposition of an extracellular matrix and cell adhesion on the scaffold structure [45]. The results from the degradation study indicated that the AlgNbgCa/ALN scaffolds remained shaped during the period analyzed, while the AlgNbgCu/ALN scaffolds degraded at a higher rate, and these findings are in agreement with a recent work [8]. It is known that cations with larger ion radius (such as Ca^{2+} ions) form a tighter structure in the egg-box model [46] compared to cations of smaller ion radius (such as Cu^{2+} ions), since they are expected to fill a larger space between the Alg chains, which may explain the slower degradation rate observed for the AlgNbgCa/ALN scaffolds compared to the AlgNbgCu/ALN scaffolds [8]. Furthermore, Ca^{2+} ions fill a larger space in the egg-box model structure, and thus it would be more difficult to be exchanged with the Na^{+} ions from the buffer medium producing a more stable matrix over time in comparison with the AlgNbgCu/ALN scaffolds [8]. According to these considerations, the study of the swelling capacity was stopped at 15 d, because the AlgNbgCu/ALN scaffolds had started their degradation process. As scaffolds are not intended to be permanent implants, the degradation rate is a critical design parameter for bone tissue regeneration in order to achieve an appropriate scaffold degradation to provide the space for matrix deposition and new tissue growth, which may ultimately lead to improved quantity and quality of regenerated bone [47]. Ideally, the degradation rate should be adjusted appropriately with the rate of tissue regeneration, so that by the time the scaffold is completely degraded, the injury is totally repaired or restored [4, 47, 48]. In addition, it is important to point out that the desired degradation rate depends on the type of injury for which the scaffold is intended as well as the site of the damage [43]. In addition, as the matrices swell and start the degradation process, the crosslinking cations are released to the medium. The fact that the AlgNbgCu/ALN scaffolds degraded faster would explain the higher levels of Cu^{2+} ions released when compared with Ca^{2+} ions released from the AlgNbgCa/ALN scaffolds during the period studied. Moreover, this relationship between the degradation process and the release profile can be noticed from day 7 onwards, where the AlgNbgCu/ALN scaffolds showed a higher degradation rate leading to a release of higher amounts of Cu^{2+} ions compared to the release of Ca^{2+} ions from the AlgNbgCa/ALN scaffolds, which were steadily released in accordance with their slow degradation rate observed. In this sense, it is important to note that results from *in vitro* cellular studies indicated that no significant differences were observed in the effects produced from extracts of the AlgNbgCu/ALN scaffolds, incubated in all the time frames studied, on HUVECs or rBMSCs. Similarly, the higher amount of ALN released from the AlgNbgCu/ALN scaffolds in each time frame studied compared to that released from AlgNbgCa/ALN could be explained by the fact that the AlgNbgCu/ALN scaffolds degraded faster than the AlgNbgCa/ALN scaffolds. In addition, it is possible to compare the percentage of ALN released from the AlgNbgCu/ALN scaffolds with their degradation percentage obtained. Hence, when ALN reached the 57 ± 12% of the amount released, the scaffolds showed a degradation percentage of 57 ± 3%, and after 2 mo, when ALN reached 89 ± 4 of the amount released, the scaffolds degraded in 95 ± 6%. In contrast, the amount of ALN released from the AlgNbgCa/ALN scaffolds was similar when compared the different time frames studied, which indicates that ALN was steadily released during the period evaluated. Moreover, Alg-crosslinked microspheres was a highly efficient system to incorporate ALN giving a 99% of encapsulation efficiency, which is higher in comparison with other microparticulated systems reported for ALN incorporation, where values for encapsulation efficiency were around 15% [49], 72% [50], 85% [51], and 92% [52, 53]. Because ALN is an expensive drug, the ability to obtain high encapsulation efficiency would avoid economic losses when derived from ALN depletion during the elaboration process of scaffolds or another drug delivery system. The effects of ALN on

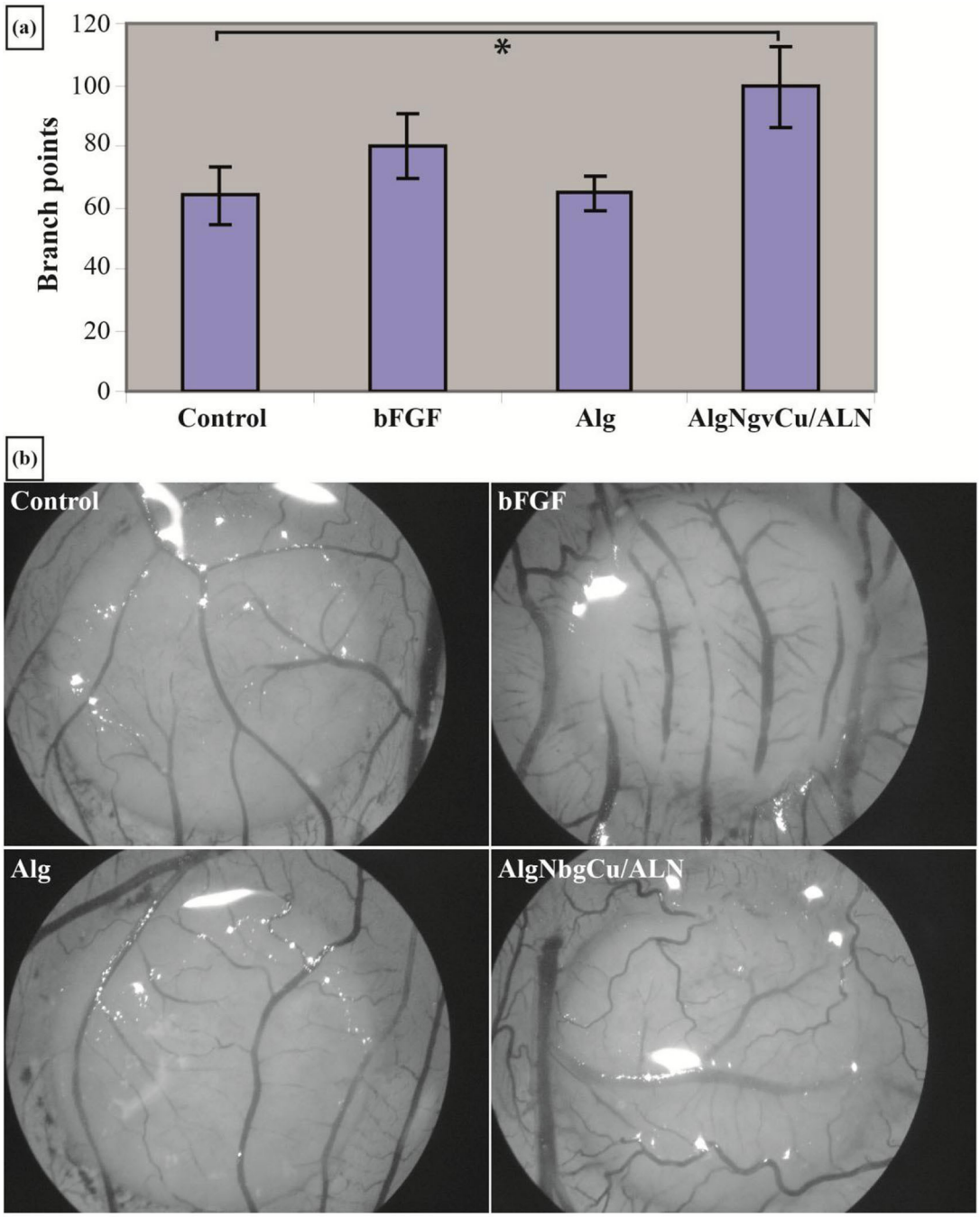

Figure 9. (a) The graphic shows the branch points formed from the AlgNbgCu/ALN, Alg, bFGF and control group. *This is significantly different ($p < 0.01$) from the control group. The data are presented as average values ±SD. (b) Pictures showing branch points formed from samples and control groups assayed. CAM in contact with 2D AlgNbgCu/ALN scaffold extracts showed higher branch-points formation.

bone and endothelial cells will be intimately related with the amount of ALN released from the matrices. Although low concentrations of ALN (10^{-8}–10^{-6} M: 3–300 ppb approximately) produce the differentiation of bone cells towards the osteogenic lineage and the proliferation of osteoblasts, as was reported previously [54–56, 57], there are some reports indicating that higher concentrations of ALN (10^{-4} M: 27 ppb approximately) are associated with favorable effects on bone-cell viability [58, 59]. Hence, these considerations allow us to explain the results from *in vitro* cellular assays, where scaffold extracts not only stimulated the proliferation of rBMSCs, but increased the ALP activity. In addition, the presence of Nbg and Cu^{2+} or Ca^{2+} ions in the scaffolds developed could produce a synergistic effect on bone tissue formation according to the properties of Nbg and the ions mentioned on bone regeneration [12]. Moreover, the results from *in vitro* cellular assays suggest that the AlgNbgCu/ALN and AlgNbgCa/ALN scaffold extracts (from all the incubation periods) produce a significant increase in the proliferation of HUVECs, and this could be attributed to two reasons. First, according to the release profile study, the concentration of ALN released from both the AlgNbgCu/ALN and AlgNbgCa/ALN scaffolds does not produce toxic effects on HUVECs. Second, the

incorporation of Nbg confers angiogenic properties to the scaffolds, as was previously mentioned about their dissolution products [36].

Furthermore, the angiogenic effects of both Cu^{2+} ions and Nbg from AlgNbgCu/ALN were evaluated by *ex vivo* assay using the CAM of quail eggs and the results indicated a significant increase in the formation of blood vessels in comparison with the effects obtained from the control group and from the Alg.

5. Conclusion

Two kind of matrices were developed, which would have different applications. Whereas Ca^{2+}-crosslinked scaffolds might be intended for bone damage requiring a longer treatment period to accomplish the complete regeneration, Cu^{2+}-crosslinked scaffolds may be applied for smaller bone defects requiring faster and more simple therapies. The size of the cation used for the alginate crosslinking impacted directly on porosity, viscoelastic properties, the degradation rate and the release profile of copper, calcium and alendronate. According to this, copper-crosslinked scaffolds showed higher values of porosity, elastic modulus, degradation rate and the amount of copper and alendronate released, when compared with calcium-crosslinked scaffolds. It is worth noting that alendronate was incorporated within the matrices with high encapsulation percentages and it was efficiently released in a controlled manner from the scaffolds. In addition, the scaffolds showed bioactivity and mechanical properties close to the endogenous trabecular bone tissue in terms of viscoelasticity. Furthermore, the scaffolds showed osteogenic and angiogenic properties on bone and endothelial cells, respectively, and the extracts of the biomaterials used promoted the formation of blood vessels in an *ex vivo* model, which indicates the potential of these matrices to be used for bone reparation and regeneration as well as their vascularization.

Acknowledgments

This work was supported by grants PICT PRH 2008-138 (financed by ANPCyT, Argentina), the Bilateral Cooperation Project between the University of Buenos Aires and the University of Erlangen-Nuremberg (financed by MINCyT—Argentina—and BMBF—Germany), the PIP 2012-2014 GI. 11220110100739 (financed by CONICET, Argentina) and partially by the 'Emerging Fields Initiative' of the University of Erlangen-Nuremberg, Germany (Project TOPbiomat).

References

[1] Langer R and Vacanti J P 1993 *Tissue Eng. Sci.* **260** 920–6
[2] Mouriño V, Cattalini J P, Roether J A, Dubey P, Roy I and Boccaccini A R 2013 Composite polymer-bioceramic scaffolds with drug delivery capability for bone tissue engineering *Expert Opin. Drug Deliv.* **10** 1353–65
[3] Chen W, Tabata Y and Tong Y W 2010 Fabricating tissue engineering scaffolds for simultaneous cell growth and drug delivery *Curr. Pharm. Des.* **16** 2388–94
[4] Garg T, Singh O, Arora S and Murthy R S R 2012 Scaffold: a novel carrier for cell and drug delivery *Crit. Rev. Ther. Drug Carrier Syst.* **29** 1–63
[5] Samorezov J E and Alsberg E 2015 Spatial regulation of controlled bioactive factor delivery for bone tissue engineering *Adv. Drug Deliv. Rev.* **84** 45–67
[6] Mouriño V, Cattalini J P and Boccaccini A R 2012 Metallic ions as therapeutic agents in tissue engineering scaffolds: an overview of their biological applications and strategies for new developments *J. R. Soc. Interface* **9** 401–19
[7] Harris G M, Rutledge K, Cheng Q, Blanchette J and Jabbarzadeh E 2013 Strategies to direct angiogenesis within scaffolds for bone tissue engineering *Curr. Pharm. Des.* **19** 3456–65
[8] Cattalini J P, Hoppe A, Pishbin F, Roether J, Boccaccini A R, Lucangioli S and Mouriño V 2015 Novel nano-composite biomaterials with controlled copper/calcium release capability for bone tissue engineering multifunctional scaffolds *J. R. Soc.* **12** 0509
[9] Mouriño V, Newby P, Pishbin F, Cattalini J P, Lucangioli S and Boccaccini A R 2011 Physicochemical, biological and drug-release properties of gallium crosslinked alginate/nanoparticulate bioactive glass composite films *Soft Matter* **7** 6705–12
[10] Erol M, Mouriño V, Newby P, Chatzistavrou X, Roether J, Hupa L and Boccaccini A R 2012 Copper-releasing, boron-containing bioactive glass-based scaffolds coated with alginate for bone tissue engineering *Acta Biomater.* **8** 792–801
[11] Cattalini J P, García J, Boccaccini A R, Lugangioli S and Mouriño V 2013 A new calcium releasing nano-composite biomaterial for bone tissue engineering scaffolds *Proc. Eng.* **59** 78–84
[12] Wu C, Zhou Y, Xu M, Han P, Chen L, Chang J and Xiao Y 2013 Copper-containing mesoporous bioactive glass scaffolds with multifunctional properties of angiogenesis capacity, osteostimulation and antibacterial activity *Biomaterials* **34** 422–33
[13] Gérard C, Bordeleau L, Barralet J and Doillon C 2010 The stimulation of angiogenesis and collagen deposition by copper *Biomaterials* **31** 824–31
[14] Li S, Xie H, Li S and Kang Y J 2012 Copper stimulates growth of human umbilical vein endothelial cells in a vascular endothelial growth factor-independent pathway *Exp. Biol. Med.* **237** 77–82
[15] Mouriño V, Cattalini J P, Lee W, Boccaccini A R and Lucangioli S 2013 Multifunctional scaffolds for bone tissue engineering and *in situ* drug delivery *Tissue Engineering Using Ceramics and Polymers* ed A R Boccaccini and P Ma (Cambridge: Woodhead) pp 648–74
[16] Mouriño V and Boccaccini A R 2010 Bone tissue engineering therapeutics: controlled drug delivery in three-dimensional scaffolds *J. R. Soc. Interface* **7** 209–27
[17] Subbiah R, Hwang M P, Van S, Do S, Park H, Lee K, Kim S H, Yun K and Park K 2015 Osteogenic/angiogenic dual growth factor delivery microcapsules for regeneration of vascularized bone tissue *Adv. Healthcare Mater.* **4** 1982–92
[18] Silverman S L and Maricic M 2007 Recent developments in bisphosphonate therapy *Semin. Arthritis Rheum.* **37** 1–12
[19] Drake M T, Clarke B L and Khosla S 2008 Bisphosphonates: mechanism of action and role in clinical practice *Mayo Clin. Proc.* **83** 1032–45
[20] Ezra A and Golomb G 2000 Administration routes and delivery systems of bisphosphonates for the treatment of bone resorption *Adv. Drug Deliv. Rev.* **42** 175–95
[21] Cremers S and Papapoulos S 2011 Pharmacology of bisphosphonates *Bone* **49** 42–9
[22] Su K, Shi X, Varshney R and Wang D 2011 Transplantable delivery systems for *in situ* controlled release of bisphosphonate in orthopedic therapy *Expert Opin. Drug Deliv.* **8** 113–26
[23] Cattalini J P, Boccaccini A R, Lucangioli S and Mouriño V 2012 Bisphosphonate-based strategies for bone tissue engineering and orthopedic implants *Tissue Eng.* B **18** 323–40

[24] Ossipov D A 2015 Bisphosphonate-modified biomaterials for drug delivery and bone tissue engineering *Expert Opin. Drug Deliv.* **12** 1443–58
[25] Brunner T J, Grass R N and Stark W J 2006 Glass and bioglass nanopowders by flame synthesis *Chem. Commun.* **13** 1384–6
[26] Vargas G E, Haro Durand L A, Cadena V, Romero M, Vera Mesones R, Mačković M, Spallek S, Spiecker E, Boccaccini A R and Gorustovich A A 2013 Effect of nano-sized bioactive glass particles on the angiogenic properties of collagen based composites *J. Mater. Sci. Mater. Med.* **24** 1261–69
[27] Das M K and Senapati P C 2008 Furosemide-loaded alginate microspheres prepared by ionic cross-linking technique: morphology and release characteristics *Indian J. Pharm. Sci.* **70** 77–84
[28] Srinivasan S, Jayasree R, Chennazhi K P, Nair S V and Jayakumar R 2012 Biocompatible alginate/nano bioactive glass ceramic composite scaffolds for periodontal tissue regeneration *Carbohydr. Polym.* **87** 274–28
[29] Kokubo T, Kim H M and Kawashita M 2003 Novel bioactive materials with different mechanical properties *Biomaterials* **24** 2161–75
[30] Baraj B, Martínez M, Sastre A and Aguilar M 1995 Simultaneous determination of Cr(III), Fe(III), Cu(II) and Pb(II) as UV-absorbing EDTA complexes by capillary zone electrophoresis *J. Chromatogr.* A **695** 103–11
[31] Cattalini J P, García J, Mouriño V and Lucangioli S 2014 Development and validation of a capillary zone electrophoresis method for the determination of calcium in composite biomaterials *Curr. Anal. Chem.* **10** 465–72
[32] Frank O, Heim M, Jacob M, Barbero A, Schäfer D, Bendik I, Dick W, Heberer M, Martin I 2002 Real-time quantitative RT-PCR analysis of human bone marrow stromal cells during osteogenic differentiation *in vitro J. Cell. Biochem.* **85** 737–46
[33] Smejkal G and Kaul C 2001 Stability of nitro blue tetrazolium-based alkaline phosphate substrates in western blotting *J. Histochem. Cytochem.* **49** 1189–90
[34] Morton R and Evans T 1992 Modification of the bicinchoninic acid protein assay to eliminate lipid interface in determining lipoprotein protein content *Anal. Biochem.* **204** 332–4
[35] Gorustovich A, Vargas G, Bretcanu O, Vera Mesones R, Porto López J and Boccaccini A R 2008 Novel bioassay to evaluate biocompatibility of bioactive glass scaffolds for tissue engineering *Adv. Appl. Ceram.* **107** 274–6
[36] Vargas G *et al* 2013 Effect of nano-sized bioactive glass particles on the angiogenic properties of collagen based composites *J. Sci. Mater. Med.* **24** 1261–9
[37] Haro Durand L, Vargas H, Romero M, Vera Mesones R, Porto López J, Boccaccini A R, Zago P, Baldi A and Gorustovich A 2015 Angiogenic effects of ionic dissolution products released from a boron-doped 45S5 bioactive glass *J. Mater. Chem.* B **3** 1142–8
[38] Tan H and Kacey G 2010 Injectable biodegradable hydrogels for tissue engineering applications *Materials* **3** 1746–67
[39] Chai C, Nissan B, Pyke S and Evans L 1995 Sol–gel derived hydroxylapatite coatings for biomedical applications *Mater. Manuf. Process.* **10** 205–16
[40] Murphy C, Haugh M and O'Brien F 2010 The effect of mean pore size on cell attachment, proliferation and migration in collagen-glycosaminoglycan scaffolds for bone tissue engineering *Biomaterials* **31** 461–6
[41] Misra S, Mohn D, Brunner T, Stark W, Philip S, Roy I, Salih V, Knowles J C and Boccaccini A R 2008 Comparison of nanoscale and microscale bioactive glass on the properties of P(3HB)/Bioglass® composites *Biomaterials* **29** 1750–61
[42] Sweeney A W, Kroon R P and Byers R K 1965 Mechanical characteristics of bone and its constituents *ASME 65-WA/HUF-7 Chicago Meeting* vol 7 pp 1–17
[43] Olszta M, Cheng X, Jee S, Kumar R, Kim Y, Kaufman M, Douglas E and Gower L 2007 Bone structure and formation: a new perspective *Mater. Sci. Eng.* R **58** 77–116
[44] Thein-Han W W and Misra R D 2009 Biomimetic chitosan-nanohydroxyapatite composite scaffolds for bone tissue engineering *Acta Biomater.* **5** 1182–97
[45] Boccaccini A R, Erol M, Stark W J, Mohn D, Hong Z and Mano J F 2010 Polymer/bioactive glass nanocomposites for biomedical applications: a review *Compos. Sci. Technol.* **70** 1764–76
[46] Grant G, Morris E, Rees D, Smith P and Thom D 1973 Biological interactions between polysaccharides and divalent cations: the egg-box model *FEBS Lett.* **32** 195–8
[47] Alsberg E, Kong H J, Hirano Y, Smith M K, Albeiruti A and Mooney D J 2003 Regulating bone formation via controlled scaffold degradation *J. Dent. Res.* **82** 903–8
[48] Woodruff M, Lange C, Reichert J, Berner A, Chen F, Fratzl P, Schantz J and Hutmacher D 2013 Bone tissue engineering: from bench to bedside *Mater. Today* **15** 430–5
[49] Mondal T, Sunny M, Khastgir D, Varma H and Ramesh P 2012 Poly (l-lactide-co-caprolactone) microspheres laden with bioactive glass-ceramic and alendronate sodium as bone regenerative scaffolds *Mater. Sci. Eng.* C **32** 697–706
[50] Kim C, Yun Y, Lee H, Hwang Y, Kwon I and Lee S 2010 *In situ* fabrication of alendronate-loaded calcium phosphate microspheres: controlled release for inhibition of osteoclastogenesis *J. Control. Release* **147** 45–53
[51] Cruz L, Assumpção E, Stanisçuaski Guterres S and Raffin Pohlmann A 2009 High encapsulation efficiency of sodium alendronate in eudragit S100/HPMC blend microparticles *Quim. Nova* **32** 1170–4
[52] Shi X, Wang Y, Ren L, Gong Y and Wang D 2009 Enhancing alendronate release from a novel plga/hydroxyapatite microspheric system for bone repairing applications *Pharm. Res.* **26** 422–30
[53] Villars F, Bordenave L, Bareille R and Amédée J 2000 Effect of human endothelial cells on human bone marrow stromal cell phenotype: role of VEGF? *J. Cell. Biochem.* **79** 672–85
[54] Ribeiro V, Garcia M, Oliveira R, Gomes P, Colaco B and Fernandes M 2014 Bisphosphonates induce the osteogenic gene expression inco-cultured human endothelial and mesenchymal stem cells *J. Cell. Mol. Med.* **18** 27–37
[55] Plotkin L, Manolagas S and Bellido T 2006 Dissociation of the pro-apoptotic effects of bisphosphonates on osteoclasts from their anti-apoptotic effects on osteoblasts/osteocytes with novel analogs *Bone* **39** 443–52
[56] Xiong Y, Yang H, Feng J, Shi Z and Wu L 2009 Effects of alendronate on the proliferation and osteogenic differentiation of MG-63 cells *J. Int. Med. Res.* **37** 407–16
[57] Chang C, Wang C, Chang J, Hsu C and Ho M 2014 The susceptive alendronate-treatment timing and dosage for osteogenesis enhancement in human bone marrow-derived stem cells *PLoS One* **9** e105705
[58] Fan C, Zhao J, Zhao B, Zhang S and Miao J 2009 Novel complex of copper and a salicylaldehyde pyrazole hydrazone derivative induces apoptosis through up-regulating integrin β4 in vascular endothelial cells *Chem. Res. Toxicol.* **22** 1517–25
[59] Kang A *et al* 2012 Up-regulation of inhibitors of DNA binding/differentiation gene during alendronate-induced osteoblast differentiation *Arch. Gynecol. Obstet.* **285** 1331–8